Chapter 18

Physics of Photodynamic Therapy

Steen J. Madsen

Introduction

Photodynamic therapy (PDT) uses light-activated drugs (photosensitizers) for the treatment of neoplastic and non-neoplastic diseases. Administration of the photosensitizer constitutes the first step in the PDT process. Then, following a waiting period (minutes to days) to allow for selective accumulation in the target tissue, the sensitizer is activated via light (usually from a laser) of a wavelength matching a prominent absorption resonance in the red or near-infrared part of the visible spectrum. Absorption of this light by the photosensitizer results in photochemical processes which ultimately produce the cytotoxic species (e.g., singlet molecular oxygen) responsible for the biological damage.

The beginning of photodynamic therapy (PDT) is generally attributed to Raab in 1900 [1] who noted that the combination of dyes and light of certain wavelengths was toxic to microorganisms; however, it wasn't until the 1970s that this therapeutic approach was introduced into the clinic [2, 3]. At that time PDT dosimetry was in a primitive state and it was recognized that, in order for PDT to gain clinical acceptance, a more rigorous dosimetric approach requiring a better understanding of PDT physics was required. A number of pioneering studies laying the foundation for PDT dosimetry were initiated in the 1980s. These studies focused primarily on gaining a better understanding of PDT dosimetry along with developing noninvasive (or minimally invasive) techniques for determining the three essential dosimetry components: light, photosensitizer, and oxygen. An excellent summary of the state of PDT physics in the 1980s, along with a recent update, can be found in [4] and [5], respectively.

Brian J.-F. Wong and Justus Ilgner (eds.), *Biomedical Optics in Otorhinolaryngology: Head and Neck Surgery*,
DOI 10.1007/978-1-4939-1758-7_18,

The purpose of this review is to provide an overview of the physics of PDT as it relates to dosimetry. Of the three dosimetry parameters, light interactions/propagation cannot be understood without a rudimentary knowledge of optical physics and transport theory and, as such, these topics are discussed in significant detail and they provide a good starting point for the review. Knowledge of the optical properties of biological tissues is important for predicting light distributions and their in vivo measurement is considered in section "Optical Property Measurements In Vivo." This is followed by an in-depth examination of various dosimetric approaches that can be used to predict biological response during PDT. The review concludes with an examination of dose-rate effects and associated strategies for improving PDT response.

Fundamental Light Interactions in Tissue

Knowledge of light distributions in biological tissue is critical for accurate PDT dosimetry. There are four fundamental types of interactions between light and tissue: refraction, reflection, absorption, and scattering. Reflection and refraction occur when light propagates between two different media and they are described by Fresnel's Law and Snell's law, respectively. The loss of light intensity between the interfaces is determined by the difference in refractive indices between the two media. From a practical point of view, light loss can be minimized by perpendicular light application [6].

Scattering is the most dominant interaction in tissues accounting for approximately 90–99 % of the total light attenuation [7]. This is in stark contrast to X-ray interactions in tissue where attenuation due to scattering and absorption is approximately equivalent. The dominance of light scattering in tissues makes optical imaging significantly more difficult than X-ray imaging. Light scattering can be either elastic (incident and scattered photons have the same energy) or inelastic (incident and scattered photons have different energy). In PDT applications, inelastic scattering (e.g., Brillouin and Raman) is negligible and can be ignored. The dominant elastic interactions in tissues are Rayleigh and Mie scattering: the type of interaction is determined by the ratio of the scattering particle size to the wavelength of light and the shape of the particle. Mie scattering dominates in situations where the wavelength and particle size are approximately equal, while Rayleigh scattering dominates for wavelengths much larger than the particle size. In practice, neither type of elastic scattering completely describes the situation in biological tissues and, as such, a number of closely related scattering formulations have been developed [8].

Compared to scattering, light absorption in tissues is relatively straightforward and can be described by the Beer–Lambert law [9]:

$$I = I_0 e^{-\varepsilon CL} \tag{1}$$

where I and I_0 are the transmitted and incident light intensities, respectively, ε is the molar extinction coefficient, C is the concentration of the solution, and L is the sample thickness. The Beer–Lambert Law is valid only under the following assumptions [10]: (1) the absorbing compounds are independent, (2) the concentration of the absorber is constant along the light path (generally not true in case of a complex material such as tissue), (3) atomic effects such as multiphoton absorption, optical saturation, or stimulated emission can be ignored (this is the case for the relatively low light intensities used in PDT), and (4) the incident light consists of parallel rays that traverse the sample without scattering (not the case for biological tissues). Since some of these assumptions are invalid in scattering media, the Beer–Lambert law has limited utility in biological media and, therefore, more sophisticated models of light transport are required to accurately determine the optical properties.

Light absorption in tissue is due primarily to a few highly absorbing molecules (chromophores) including water, oxyhemoglobin, deoxyhemoglobin, melanin, and cytochromes. The absorption spectra of these molecules are illustrated in Fig. 1 which shows that there is an "optical window" between 600 and 1400 nm where the absorbance of each chromophore is relatively low. This optical window provides the rationale for using red to near-infrared absorbing photosensitizers since these wavelengths have the deepest penetration in tissues.

Light Transport in Biological Tissues

Tissues are considered optically turbid since they scatter and absorb light and, as such, light propagation can be modeled using the radiation transport equation (RTE), also known as the Boltzmann transport equation [11]. Solution of the RTE requires knowledge of the fundamental optical properties (absorption, scattering, and scattering anisotropy). Once the tissue optical properties have been determined, the RTE can be used to calculate the light distribution (fluence rate) at any point for a given source geometry. Analytical solutions to the RTE exist in only a few limiting cases, thus necessitating the use of approximate methods.

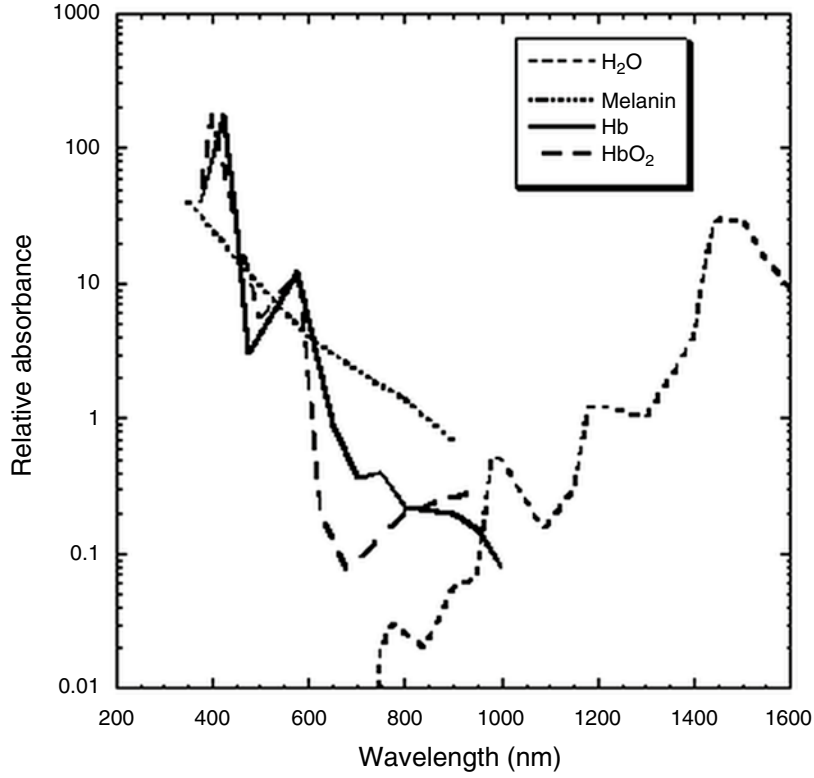

Fig. 1 Absorption spectra of common tissue chromophores. An optical window corresponding to reduced scattering and absorption is evident from 600 to 1400 nm. *Hb* hemoglobin, *HbO2* oxyhemoglobin

Radiation Transport Equation

The time-dependent RTE describing light transport in a turbid medium can be expressed as [5]:

$$\frac{1}{v}\frac{\partial}{\partial t}L(\mathbf{r},\Omega,t)+\Omega\cdot\nabla L(\mathbf{r},\Omega,t)+[\mu_a(\mathbf{r})+\mu_s(\mathbf{r})]L(\mathbf{r},\Omega,t) = \mu_s\int_{4\pi}p(\Omega,\Omega')L(\mathbf{r},\Omega',t)\mathrm{d}\Omega'+S(\mathbf{r},\Omega,t) \quad (2)$$

where $L(\mathbf{r}, \mathbf{\Omega})$ is the energy radiance which is the radiant power transported at location $\mathbf{r}$ in a given direction $\mathbf{\Omega}$ per unit solid angle per unit area perpendicular to that direction [W m^{-2} sr^{-1}]. The energy radiance is considered the fundamental quantity of interest in the RTE. The energy fluence rate, $E_0(\mathbf{r})$ [W m^{-2}], can be determined simply by integrating the radiance over 4π solid angle. This is an important parameter in a number of applications including PDT. The absorption coefficient is denoted by μ_a, while the scattering coefficient is given by μ_s. $S(\mathbf{r}, \mathbf{\Omega}, t)$ is a source term, v is the speed of light in tissue, and $p(\mathbf{\Omega},\mathbf{\Omega}')$ is the phase function which gives the probability that a photon moving in the direction of unit

vector **Ω** is scattered in the direction **Ω′**. The phase function can be expanded as a series in Legendre polynomials, *Pn* [12]:

$$p(\Omega, \Omega') = \frac{1}{4\pi} \sum_{\infty}^{n=0} (2n+1) b_n P_n(\Omega, \Omega') \qquad (3)$$

The first term accounts for normalization ($b_0 = 1$) and the second term yields $b_1 = g$, the mean cosine of the scattering angle. Accurate values for higher order terms in the expansion of the phase function are very difficult to obtain for biological tissues. The value of g varies from −1 to 1: $g = 0$ corresponds to isotroptic scattering, while values of 1 and −1 correspond to total forward and backward scattering, respectively. Light scattering in most tissues is highly forwardly directed ($g \approx 0.7$–0.9), thus requiring several scattering events to randomize the direction of light propagation. The most commonly used phase function to describe light scattering in tissues is the Henyey–Greenstein phase function which is defined by $bn = gn$ in Eq. (1) [13]. This phase function was originally developed to describe light scattering in stellar atmospheres and can be applied to biological tissue in a very straightforward manner since it only depends on one parameter (g).

Solution to the Transport Equation

Solution of the RTE assumes that the wave properties of light are ignored and therefore light photons propagating in biological tissues are considered as neutral particles, much like neutrons in a nuclear reactor. Analytical solutions to the RTE can be found in only a few limiting cases. Chandrasekhar [14] solved the case of a homogeneous, semi-infinite, isotropically scattering medium irradiated with a collimated beam of infinite extent, while Rybicki [15] solved the RTE in a similar medium irradiated with a narrow collimated beam. Due to the geometrical constraints and the simple assumptions regarding medium composition, these techniques are not relevant for clinical PDT.

Exact Solutions

Numerical Techniques: Monte Carlo Simulations

The most commonly used numerical technique for solving the RTE is Monte Carlo (MC) modeling. Although the Monte Carlo approach was introduced in the late 1940s to investigate neutron transport in various materials [16], it wasn't until the early 1980s that it was applied to tissue optics [17]. The MC technique is capable of solving the RTE to a high degree of accuracy and, as such, it has become the gold standard for modeling light propagation in tissue [18]. For example, MC simulations are commonly used to verify the accuracy of analytical models such as diffusion theory [19].

The algorithms used in MC simulations are relatively straightforward and codes for simulating light propagation in tissues are readily available (e.g., [20]). MC simulations track the history of individual photons in the medium, and parameters such as the distance between interactions and the scattering angle are sampled

from appropriate probability distributions which depend on the optical properties of the medium [17]. The fluence can be determined from the number of photon interactions recorded in each volume element. In addition to obtaining light distributions from known optical properties (the forward problem), MC modeling can also be used to estimate optical properties by fitting simulated light distributions to experimental data (the inverse problem).

The primary advantage of the MC approach is that it can be used to simulate light propagation under realistic conditions (e.g., variety of light sources, multiple tissue types, and complex geometries); however, this flexibility comes with a price: simulations can be computationally intensive as they typically require millions of photon histories to obtain the desired accuracy—the higher the degree of accuracy required, the longer the simulation time. A number of techniques have been introduced to increase the speed of MC simulations including scaling and perturbation methods, hybrid approaches, variance reduction techniques, and parallel computation methods [21]. Parallel computation methods are particularly intriguing since they have the potential to significantly reduce computation times. In essence, this approach involves running an MC simulation simultaneously on many computers with the goal of using the dead time of networked computers to increase the speed of MC simulations. A variation of this approach is to use a multiple processor MC code that can be run on one computer with multiple processors, i.e., parallelization [22]. Other techniques for increasing computation speed include (1) the implementation of MC codes in graphic processing unit (GPU) environments [23], (2) using field-programmable gate arrays [24], and (3) using Internet-based parallel computation (cloud computing) [25]. Some of these approaches have been shown to reduce computation times by a factor of 1000 compared to conventional CPU-based approaches [21].

MC modeling of light propagation in biological tissues has been used to simulate a number of common optical measurements including fluorescence and diffuse transmittance and reflectance. MC modeling is ideally suited for PDT applications since it can be used in realistic treatment situations involving multiple sources, complex geometries, and heterogeneous tissues. For example, MC simulations have been used to characterize PDT dosimetry in a variety of oncologic applications including prostate [26] and skin cancers [27–29]. In this context, MC modeling is particularly useful since it has the ability to simulate both the temporal and spatial distributions of the fundamental dosimetric PDT parameters (light distribution and photosensitizer and oxygen concentrations).

The Diffusion Approximation

Under the assumption that the radiance is only weakly direction dependent (i.e., linearly anisotropic), the integro-differential equation [Eq. (1)] can be expressed as a partial differential equation

that can be solved using standard techniques. Specifically, the radiance is expanded in terms of spherical harmonics, $Y_{n,m}$, with only the first two terms considered. In terms of the fluence rate, $E_0(\mathbf{r})$, the diffusion equation can be expressed [5]:

$$\frac{1}{v}\frac{\partial}{\partial t}E_0(\mathbf{r},t) - \nabla\cdot[3(1-g(\mathbf{r}))\mu_s(\mathbf{r})]^{-1}\nabla E_0(\mathbf{r},t) + \mu_a(\mathbf{r})E_0(\mathbf{r},t) = S(\mathbf{r},t) \quad (4)$$

In the diffusion approximation, the source-free equations are invariant for changes in μ_s and g that leave $\mu_s(1-g)$ constant [30]. Therefore, the precise value of g might not be required in regions where the diffusion approximation holds, i.e., far from boundaries and sources and in highly scattering media ($\mu_s(1-g) \gg \mu_a$). This represents a significant simplification since g is very difficult to measure. Thus, for determination of light distribution in tissues, it is sufficient to know μ_a and $\mu_s(1-g)$ accurately and g only approximately [31]. $\mu_s(1-g)$ is typically denoted by μ_s', the so-called reduced (or transport) scattering coefficient. Accurate values of g may only be important close to boundaries and sources, i.e., under conditions where the diffusion approximation is invalid. In such instances, alternative approximation methods are required, e.g., higher-order analytic solutions using spherical harmonics for the angular parameters in Eq. (1) and expansion of the phase function in Legendre polynomials [Eq. (3)] [32]. Analytic solutions to the diffusion equation exist only for very simple conditions (optically homogeneous tissue) and geometries (infinite, semi-infinite, and slab) [33].

Other Approximation Methods

Kubelka and Munk developed a simple two-flux model to describe the propagation of a uniform diffuse irradiance in a one-dimensional slab with no reflection at the boundaries [34, 35]. It is assumed that the slab is illuminated by a Lambertian source and that the radiance remains isotropic with depth. The model has been used primarily for determining the optical properties of tissues in simple layered models; however, the underlying assumptions of isotropic scattering, matched boundaries, and diffuse irradiance are unrealistic for many light-tissue applications.

The inverse adding doubling (IAD) technique is a numerical solution to the one-dimensional RTE that is applicable to homogeneous turbid slabs with any optical thickness, albedo, or phase function [36–38]. The method is a reversal of the usual procedure of calculating reflection and transmission from optical properties, hence the term "inverse." The IAD approach is ideally suited to measurements involving biological tissues placed between glass slides, and it has been used to determine the optical properties of a wide variety of tissues. Since this technique applies only to uniformly illuminated homogenous slabs, it is difficult to envision its use for in vivo determination of optical properties.

Optical Property Measurements In Vivo

A number of methods have been employed to measure the optical properties of biological tissues. These include direct methods requiring tissue samples sufficiently thin such that single scattering dominates. This requires measurements on excised tissues. Unfortunately, the results are fraught with uncertainty due to preparation and handling artifacts such as blood loss and freezing/thawing. These types of measurements are ill suited to the clinic since they are time intensive and cannot be used for real-time optical property monitoring during PDT. For these reasons, the focus has been on in vivo measurements using either invasive or noninvasive approaches. Invasive methods involve the insertion of fiber optic sources and detectors directly into the tissue of interest for measurements of the light distribution. A model of light propagation in a homogeneous medium is then employed to estimate the interaction coefficients from a set of measurements (e.g., the fluence rate at a number of distances from the internal source). Such measurements are commonly employed in PDT. In noninvasive approaches, the sources and detectors are placed in contact with the external boundary. Although this is less intrusive, the accuracy of the optical properties is often difficult to estimate since the light travels through different tissue types.

Spectroscopic techniques for in vivo determination of tissue optical properties can be divided into three categories: steady-state (or continuous wave), time-resolved, and frequency domains. In the vast majority of cases, the diffusion approximation is used to extract the optical properties (μ_a and μ_s').

Steady-State Spectroscopy

Reflectance Measurements

In diffuse reflectance measurements, light is collected by a detector fiber at a known distance from a source fiber (Fig. 2a). Both fibers are placed in contact with the surface of the medium and the measured reflectance is fitted to a model of light propagation (i.e., the diffusion approximation) in order to extract the optical properties of the medium. Nonlinear least squares fitting routines (e.g., Levenberg–Marquardt algorithm) are commonly used to fit the measured data to the model [39]. Analytic expressions based on the diffusion approximation have been derived by a number of groups applicable in simple geometries such as semi-infinite homogeneous media [19, 40, 41]. Using the diffusion theory solution of Kienle and Patterson [41], the diffuse reflectance as a function of fiber separation (ρ) is given by

$$R(\rho) = C_1\psi(\rho) + C_2 j_z(\rho) \tag{5}$$

where $\psi(\rho)$ is the fluence rate at the surface and $jz(\rho)$ is the reflected flux exiting the surface from the tissue. C_1 and C_2 are constants which depend on the relative refractive index mismatch at the tissue/detector interface and the numerical aperture of the detection fibers.

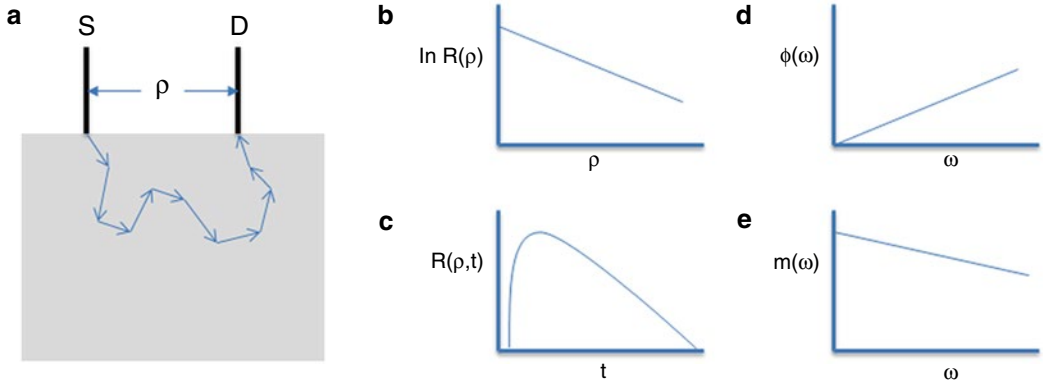

Fig. 2 Noninvasive spectroscopic approaches for determining optical properties. (**a**) Photons are introduced into a homogeneous semi-infinite tissue-like medium via an optical fiber (S) and detected by an optical fiber (D). In the steady-state approach (**b**), diffusely reflected photons are collected as a function of source-detector fiber separation (ρ). In time-resolved spectroscopy (**c**), diffusely reflected photons are detected as a function of time. In the frequency domain, the phase shift (ϕ) (**d**) and demodulation amplitude (m) (**e**) are determined as a function of modulation frequency (ω). In all cases, the tissue optical properties (μ_a and μ_s') can be determined by fitting the diffusion approximation to the experimental data illustrated in (**b**)–(**e**)

If the index of refraction of tissue is 1.4, the numerical aperture of the detection fiber is 0.22, and if the index of refraction of the detector fiber is 1.46, then C_1 is 1.46 and C_2 is 0.0389 [42]. In Eq. (5), $\psi(\rho)$ and $jz(\rho)$ are given by

$$\psi(\rho) = \frac{1}{4\pi D}\left(\frac{\exp(-\mu_{\text{eff}} r_1(\rho))}{r_1(\rho)} - \frac{\exp(-\mu_{\text{eff}} r_2(\rho))}{r_2(\rho)}\right) \tag{6}$$

and

$$j_z(\rho) = \frac{1}{4\pi\mu_t'}\left[\left(\mu_{\text{eff}} + \frac{1}{r_1(\rho)}\right)\frac{\exp(-\mu_{\text{eff}} r_1(\rho))}{r_1^2(\rho)} + \left(\frac{1}{\mu_t'} + 2z_b\right)\left(\mu_{\text{eff}} + \frac{1}{r_2(\rho)}\right)\frac{\exp(-\mu_{\text{eff}} r_2(\rho)}{r_2^2(\rho)}\right] \tag{7}$$

where D is the diffusion coefficient ($=[3(\mu_a + \mu_s')]^{-1}$), μ_{eff} is the effective attenuation coefficient ($=[3\mu_a(\mu_a + \mu_s')]^{1/2}$), and μ_t' is the total interaction coefficient ($=\mu_a + \mu_s'$). The parameter z_b is the extrapolated boundary position, i.e., the location of an imaginary boundary a distance of $2AD$ above the surface of the medium, where A is a dimensionless constant determined by the relative refractive index mismatch at the boundary [40]. The parameter $r_1(\rho)$ is the distance from a detection point on the surface of the medium to an imaginary point source located one transport mean free path ($=1/\mu_t'$) directly below the source fiber, while $r_2(\rho)$ is the distance from the detection point on the surface to a negative image source located at a distance of $1/\mu_t' + 2z_b$ directly above the source fiber. The rationale for using these parameters is discussed in detail in [40]. The use of reflectance measurements and steady-state

diffusion theory has been shown to yield values of μ_a and μ_s' to an accuracy of around 10 %.

Equation (18.5) applies to a semi-infinite homogeneous medium. Solutions to the diffusion equation in the steady-state, time, and frequency domains have also been derived for two-layered turbid media with an infinitely thick second layer [43].

Interstitial Measurements

Both source and detector fibers are inserted into the medium and the fluence rate is measured as a function of radial distance between the fibers. Due to the limited penetration depth of light in biological tissues, the medium is typically considered infinite in extent and, as such, boundary conditions can be ignored and the solution to the diffusion equation is thus relatively trivial. In this case, the fluence rate ϕ at a distance r around an isotropic point source delivering a radiant power P into the infinite turbid medium is given by [44]:

$$\phi(r) = \frac{P}{4\pi Dr} \exp(-\mu_{\text{eff}} r) \tag{8}$$

The equation can be modified to account for tissue heterogeneity and extended sources [45].

Time-Resolved Spectroscopy

In time-resolved (or time-of-flight) spectroscopy, the temporal spreading of a short light pulse ($\leq 10^{-12}$ s) is measured in reflectance or transmittance mode as it travels through a scattering medium such as tissue (Fig. 2c). The temporal spreading of the light pulse is related to the optical properties of the medium which may be extracted via application of a model of light propagation. For example, the time-dependent diffusion equation has been solved for semi-infinite and finite homogeneous tissue slabs [46] as well as spherical and cylindrical geometries [47]. A particularly useful quantity is the time-resolved diffuse reflectance from a homogeneous semi-infinite tissue slab:

$$R(\rho,t) = (4\pi Dc)^{-3/2} z_0 t^{-5/2} \exp(-\mu_a ct) \exp\left(-\frac{\rho^2 + z_0^2}{4Dct}\right) \tag{9}$$

where ρ is the source–detector fiber separation, c is the speed of light in tissue (=0.214 mm ps^{-1} assuming that $n = 1.4$), and z_0 is the depth at which the incident photons are initially scattered ($= 1/\mu_s'$). Time-resolved spectroscopy has been investigated in a wide variety of geometries [43, 46, 48] and the accuracy of the derived optical properties (μ_a and μ_s') is similar to that obtained with steady-state techniques ($\approx$10 %). The high cost of instrumentation required for time-resolved spectroscopy is a significant limitation.

Frequency Domain Spectroscopy

In frequency domain spectroscopy the intensity of light incident on biological tissue is modulated at a high frequency (10^8–10^9 Hz)

and the diffusely reflected or transmitted signal is measured with a phase-sensitive detector (Figs. 2d,e). It has been shown that intensity-modulated light propagates through multiple scattering media as diffuse photon density waves with a coherent front [49–51]. Since density wave dispersion is a function of the optical properties of the material interrogated, the absorption and transport scattering coefficients can be determined simply by fitting the measured frequency and distance-dependent behavior to analytical expressions derived from diffusion theory [40, 51, 52]. For example, Fourier transformation of Eq. (18.9) yields analytic expressions for the modulation and phase as functions of the optical properties of the tissue.

Compared to time-resolved techniques, frequency domain spectroscopy offers several advantages including (1) cheaper instrumentation, especially for frequencies below 200 MHz [53, 54], (2) the possibility of determining the optical properties (μ_a and μ_s') from modulation and phase measurements at a single frequency, and (3) the potential of monitoring dynamic phenomena (e.g., hemoglobin oxygenation) since both modulation and phase can be measured over short time periods. For these reasons, frequency domain spectroscopy has become the preferred method for diffuse optical spectroscopy applications.

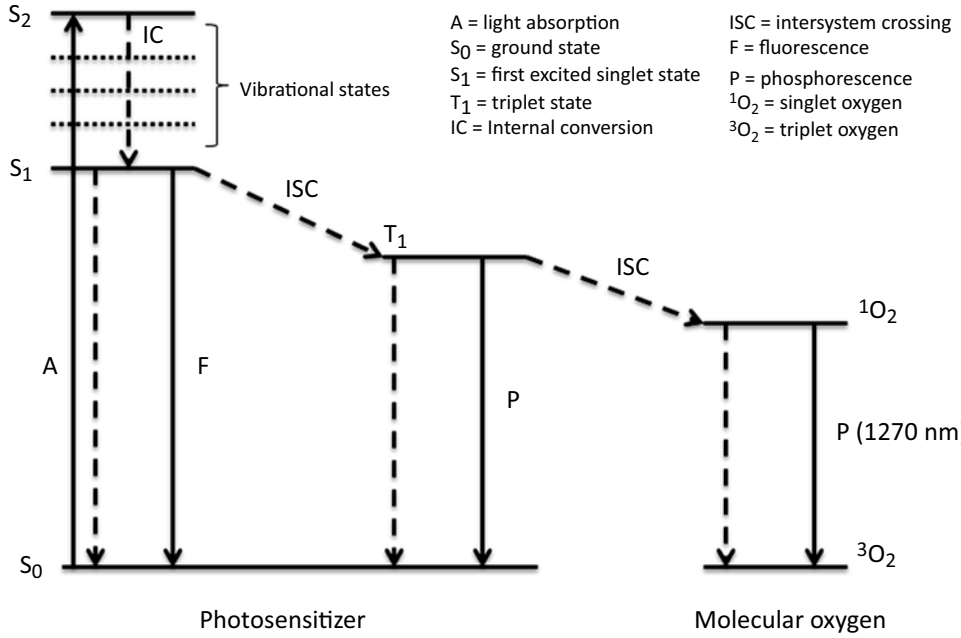

Fig. 3 Abbreviated Jablonski diagram showing the most relevant energy levels and transitions for singlet oxygen-mediated PDT. *Solid* and *dashed arrows* denote radiative and non-radiative transitions, respectively. De-excitation of singlet molecular oxygen to ground-state triplet molecular oxygen is accompanied by 1270 nm phosphorescence which can be used as a direct dose metric during PDT

PDT Dosimetry

Introduction

In comparison to ionizing radiation, PDT dosimetry is not well developed. This can be attributed to the complexity of the PDT process which is illustrated in Fig. 3. A photosensitizer in its ground state is characterized by paired electrons with a total spin $(S) = 0$ and a corresponding spin multiplicity of 1. This ground-state configuration is termed a singlet state (S_0). Upon absorption of photons of appropriate energy, the photosensitizer is raised to an electronically excited singlet state Sn ($n = 1, 2, 3\ldots$) which contains additional vibrational modes. The photosensitizer may return to its ground state resulting in prompt fluorescence emission; however, efficient photosensitizers typically undergo an intersystem crossing (ISC) through rearrangement of electronic spin resulting in a triplet excited state (T_1). This triplet state has a relatively long lifetime in biological tissues (typically tens of microseconds) and, in well-oxygenated conditions, de-excites via energy transfer to ground-state molecular oxygen in a triplet state ($^3O_2$). If sufficient energy is provided in this transfer, singlet excited oxygen $^1O_2$ is produced. For example, typical sensitizers yield approximately one molecule of singlet oxygen for every two photons absorbed [55]. There is strong evidence showing that singlet oxygen is the primary cytotoxic species in PDT [56, 57]; however, reactions yielding other reactive species have also been demonstrated [58]. PDT-induced tissue necrosis requires the production of approximately 10^{18}–10^{19} molecules $cm^{-3}$of singlet oxygen [59].

Clinical PDT dosimetry has traditionally been accomplished based on the amount of photosensitizer administered followed by measurement of the incident light exposure. This is a very simplistic and inadequate approach due to intra- and inter-patient variability in sensitizer concentrations. Second, the light distribution is dependent on the optical properties of the target tissue. Third, the yield of singlet oxygen depends on the oxygenation state of the tissue. Finally, the photosensitizer concentration, light distribution, and tissue oxygenation may change during treatment and one parameter may interact with the other. These factors must be accounted for in a successful PDT dosimetry scheme.

Assuming that singlet oxygen is responsible for the biological response, Wilson et al. [60] have proposed three dosimetry approaches:

1. Explicit dosimetry which typically involves separate measurements of light, photosensitizer, and oxygen during PDT. These measurements are then incorporated into a dose model. Although this is a cumbersome approach fraught with uncertainties, it has nevertheless been used by a number of groups [61–63].

2. Implicit dosimetry in which a combination of treatment parameters are incorporated into a single dose metric, e.g., photosensitizer photobleaching which can be determined by monitoring photosensitizer fluorescence during PDT. Fluorescence spectroscopic measurements of photoproducts associated with photobleaching have also been proposed as an implicit dosimetry technique [64–66].
3. Direct dosimetry in which the cytotoxic species, single oxygen, is measured.

Strategies for measuring the individual components (light photosensitizer and oxygen) required for explicit dosimetry will be summarized in sections "Light Dosimetry," "Photosensitizer Dosimetry," and "Oxygen Dosimetry," while implicit dosimetry techniques and direct singlet oxygen measurements will be discussed in sections "Implicit Dosimetry" and "Direct Dosimetry," respectively.

Light Dosimetry

Determination of light fluence was discussed in section "Light Transport in Biological Tissues." It was shown that the fluence (and fluence rate) can be determined from knowledge of the tissue optical properties and the irradiation geometry. Another approach involves the direct measurement of the fluence rate which is typically accomplished at discrete points within the tissue. Rather than generating a complete fluence rate profile, which would require many invasive measurements, the goal is usually to verify the results of calculations and/or to determine the fluence rate at clinically critical locations where calculations may be suspect (e.g., near boundaries). Measurements are typically accomplished using small diameter (≈200 μm-dia.) optical fibers with isotropic scattering tips. Using commercially available fiber probes with highly uniform angular response (±5 %), fluence rate measurements can be made with an accuracy of around 5–10 % [5].

Photosensitizer Dosimetry

A number of approaches have been used to measure photosensitizer concentration in tissues. The most promising techniques involve optical methods based on absorption, fluorescence, or Raman scattering which can yield the concentration at discrete points or the mean concentration over a tissue volume.

Since most photosensitizers fluoresce, the fluorescence emission from a tissue can be used to infer the concentration of the photosensitizer. The relationship between emission and concentration is not straightforward since the emission may be affected by the local environment of the photosensitizer including pH. Another complication is that both the excitation and emission light typically propagate through thick tissue layers and, therefore, the detected fluorescence will depend on the tissue optical properties. This

effect can be minimized by delivering the excitation light and collecting the fluorescence via an optical fiber inserted directly into the tissue [67]. Although this approach is capable of yielding photosensitizer concentrations to an accuracy of about 10 %, it is limited by the small tissue volumes sampled. Larger sample volumes have been accomplished using surface probes consisting of fiber bundles [68].

In the case of non-fluorescing or low quantum yield photosensitizers, absorption spectroscopy is commonly used. The objective is to determine the photosensitizer concentration from its specific contribution to the total absorption coefficient. This is typically accomplished by determining the absorption coefficient over a range of wavelengths so that the sensitizer peaks can be differentiated from the tissue background absorption. A system for performing quantitative absorption spectroscopy to estimate photosensitizer concentration in vivo has been described by Farrell et al. [69].

A number of other approaches have been developed for quantifying sensitizer concentration. The most promising of these is Raman scattering which has been used for ex vivo measurements [70], although fiber optic-based Raman systems developed for in vivo diagnostics could be used for this purpose.

Oxygen Dosimetry

In situ measurements of tissue oxygenation require thin probes. Commercially available metal-based microelectrodes for measuring pO_2 in tissues have tip diameters of a few μm [71]. Although these microelectrodes are capable of measuring pO_2 with excellent spatial and temporal resolution, they are rather fragile and can easily be broken during clinical measurements. Similar to fluence rate measurements discussed in section "Light Dosimetry," pO_2 measurements are made at discrete points in the tissue and therefore placement of electrodes requires careful consideration of the tissue to be monitored. A combination fiber optic probe for measuring pO_2, pCO_2, and pH was approved for clinical use in 2000 [71]. Advantages of these luminescence-based sensors include their nonchemical and reversible mechanism of sensing in which both the probe and the analyte are not consumed, high sensitivity and selectivity, rapid response times (ms), and the possibility of contactless measurements through a (semi) transparent material [72]. Additionally, due to their larger tip diameters (ca. 500 μm), optical probes are also more robust. Some studies have found that the larger fiber optic probes consistently measure a higher fraction of hypoxic pO_2 values in both tumors and normal tissues compared to microelectrodes [73]. This may be due to damage to the microcirculation by the larger optic probes.

Although direct microelectrode/fiber optic measurements of tissue oxygenation have not been attempted during clinical PDT, spectroscopic techniques, such as those described in section "Optical Property Measurements In Vivo," have been investigated. For example,

Zhu et al. [63] used a continuous wave spectroscopy approach (section "Interstitial Measurements") to measure both oxy- and deoxyhemoglobin concentrations in human prostate during PDT. Knowledge of these parameters allows evaluation of tissue oxygenation.

Implicit Dosimetry

In most instances, implicit dosimetry is accomplished via detection of photobleaching or photoproducts. In this context, photobleaching refers to the photochemical destruction of the sensitizer rendering it incapable of further fluorescence. For some photosensitizers, photobleaching is mediated by $^1O_2$ and, therefore, it should be possible to infer its concentration based on the initial and final sensitizer concentrations. For example, Dysart and Patterson [74] have developed an expression for the total amount (i.e., dose) of singlet oxygen generated during a PDT treatment starting at $t=0$ and ending at $t=T$:

$$\text{Dose} = \frac{1}{\tau}\int_T^0 [^1O_2]dt = \frac{1}{\tau\ k_{os}}\log_e \frac{[S_0]_{t=0}+\gamma}{[S_0]_{t=T}+\gamma} \qquad (18.10)$$

where τ_Δ is the singlet oxygen lifetime in the tissue, k_{os} is the sensitizer bleaching rate constant, and γ is the effective minimum sensitizer concentration. Therefore, only a few parameters are required to determine the absolute dose, namely, the initial and final sensitizer concentrations, $[S_0]t_{=0}$ and $[S_0]t_{=}T$, and τ_Δ, k_{os}, and γ.

This model has been verified in simple in vitro systems using the sensitizer mTHPC. The model is accurate only under well-oxygenated conditions ($pO_2 > 5$ μM) [75] and it cannot be applied to commonly used photosensitizers such as Photofrin and ALA-PpIX since they can be photobleached by non-$^1O_2$ pathways under hypoxic conditions [74, 76, 77]. The results of these studies suggest that there are likely two different photobleaching mechanisms for sensitizers such as Photofrin: one mediated by singlet oxygen and the other by the sensitizer triplet state. The relative importance of each depends on the ambient oxygen concentration. Furthermore, it has been postulated that the fluorescent photoproduct of Photofrin is due exclusively to singlet oxygen-mediated bleaching and, as such, determination of the concentration of the photoproduct would be more reliable than measuring Photofrin photobleaching [76]. Similarly, the photoproducts of PpIX [77] and BPD [64] have been found to be more reliable predictors of PDT response in vitro and in vivo.

In summary, implicit dosimetry is still in its infancy: the majority of studies have been performed in relatively simple systems consisting of cell suspensions and multicell spheroids. Additional in vivo studies will be required in order to determine the clinical potential of this approach.

Direct Dosimetry

Direct dosimetry involves measurement of the 1270 nm phosphorescence resulting from the de-excitation of singlet oxygen to its ground state. Although measurement of this signal is trivial in vitro, its detection in complex media such as biological tissue is challenging due to its short lifetime (30–200 ns) and weak emission. As a result, singlet oxygen luminescence detection requires sensitive and rapid time response detection systems. Early systems employing liquid nitrogen-cooled germanium detectors and lock-in detection techniques were capable of measuring singlet oxygen luminescence in cell suspensions, but lacked the sensitivity for reliable measurements in vivo [78–80]. With the introduction of sensitive near-infrared photomultiplier tubes in the late 1990s, in vivo singlet oxygen detection became possible and two groups reported positive results in animals [57, 81]. In subsequent studies, Niedre et al. [82] showed that the total singlet oxygen signal detected during PDT of tumor cell suspensions correlated well with cell survival over a wide range of treatment conditions. These results have been confirmed in animals which also show a good correlation between cumulative singlet oxygen signals and biological response [83]. There are no reports of measurements during PDT in humans even though this is highly feasible for easily accessible lesions such as skin cancers.

Even with state-of-the-art instrumentation, singlet oxygen luminescence detection is difficult. This is due to a combination of factors including the weakness of the luminescence and the low quantum efficiency (~1 %) of the detectors [75]. As a result, the luminescence is difficult to measure since the overall signal also contains stronger sources of luminescence, including photosensitizer and cell tissue fluorescence [84]. Due to the low signal, fiber optic probes cannot be used to collect the singlet oxygen luminescence and acceptable signal-to-noise ratios can only be obtained by integrating the signal over a significant volume of irradiated tissue [5]. In addition, the instrumentation is very complex and significantly more expensive compared to that required for continuous wave fluorescence measurements in the visible spectrum.

Dose-Rate Effects

The biological response to PDT depends not only on light fluence but also on the rate at which light is delivered. Dose-rate effects may be due to biological and/or physical mechanisms. As fluence rates are reduced (corresponding to longer treatment times), cell repair and responses to oxidative stress become important [85–87]. Additionally, physical mechanisms involving photosensitizer ground-state depletion during pulsed irradiation and fluence-rate-dependent photochemical oxygen depletion are also important factors influencing biological response to PDT.

PDT with short-pulse lasers has been shown to be less effective compared to continuous wave irradiation for equivalent average fluence rates [88]. This is attributed to the finite number of

sensitizer molecules in the tissue volume. If a significant fraction of these is excited during the initial part of the laser pulse, photons in the remainder of the pulse will be wasted due to the reduced likelihood of absorption and subsequent singlet oxygen production.

Oxygen depletion, the second physical mechanism for dose-rate effects, typically occurs on a timescale of seconds and depends on the average fluence rate. Simply stated, oxygen depletion occurs when PDT-induced photochemical oxygen consumption exceeds the ability of the microvasculature to deliver oxygen to the irradiated tissue. Tromberg et al. [89] were the first to show that oxygen concentration was reversibly reduced during PDT irradiation. Subsequently, biophysical models have shown that oxygen depletion is likely under typical PDT treatment conditions [90, 91]. These modeling studies have been verified by a number of other groups [92–95]. There is now substantial evidence that PDT is less effective at high fluence rates [66, 90, 92, 96, 97].

Delivery of light and/or photosensitizer at very low dose rates is a potential strategy for overcoming the ineffectiveness of PDT at high fluence rates. This has been termed metronomic PDT (mPDT) [98] and must be distinguished from treatments in which the light dose rate is only slightly reduced (by a factor of 2 or 3) in order to avoid oxygen depletion. Metronomic PDT using ALA in a rat brain tumor model has been shown capable of producing tumor cell (glioma) killing through apoptosis without inducing any measurable damage to normal brain. Furthermore, no necrotic cell death was found in the tumor. This is a particularly interesting observation since necrotic cell death triggers inflammatory responses which may result in additional secondary damage to normal brain. With regard to intracranial treatments, another rationale for mPDT is that single high dose-rate PDT treatments are unlikely to result in the delivery of a tumoricidal dose beyond about 2 cm with current photosensitizers. This is due to an inability to deliver a sufficiently high light dose at depth in a clinically acceptable treatment time, especially when PDT is given intraoperatively to the surface of the resection bed. However, delivering the light over a much longer period (hours, days, or weeks) relaxes this constraint. Such a protracted delivery scheme requires specialized indwelling applicators such as those used for intracranial brachytherapy (Fig. 4a, b) [99].

The low dose-rate PDT regime has been explored extensively in vitro using human glioma spheroids [100]. Specifically, enhanced efficacy of ALA-PDT at $\leq$10 mW cm^{-2} was demonstrated and repetitive low fluence rate treatments resulted in much higher tumor cell kill than single treatments (Fig. 4c). Collectively, the photobiological findings from the mPDT and low dose-rate studies provide a compelling rationale for investigating low and very low dose rate PDT, especially for the treatment of high-grade glioma.

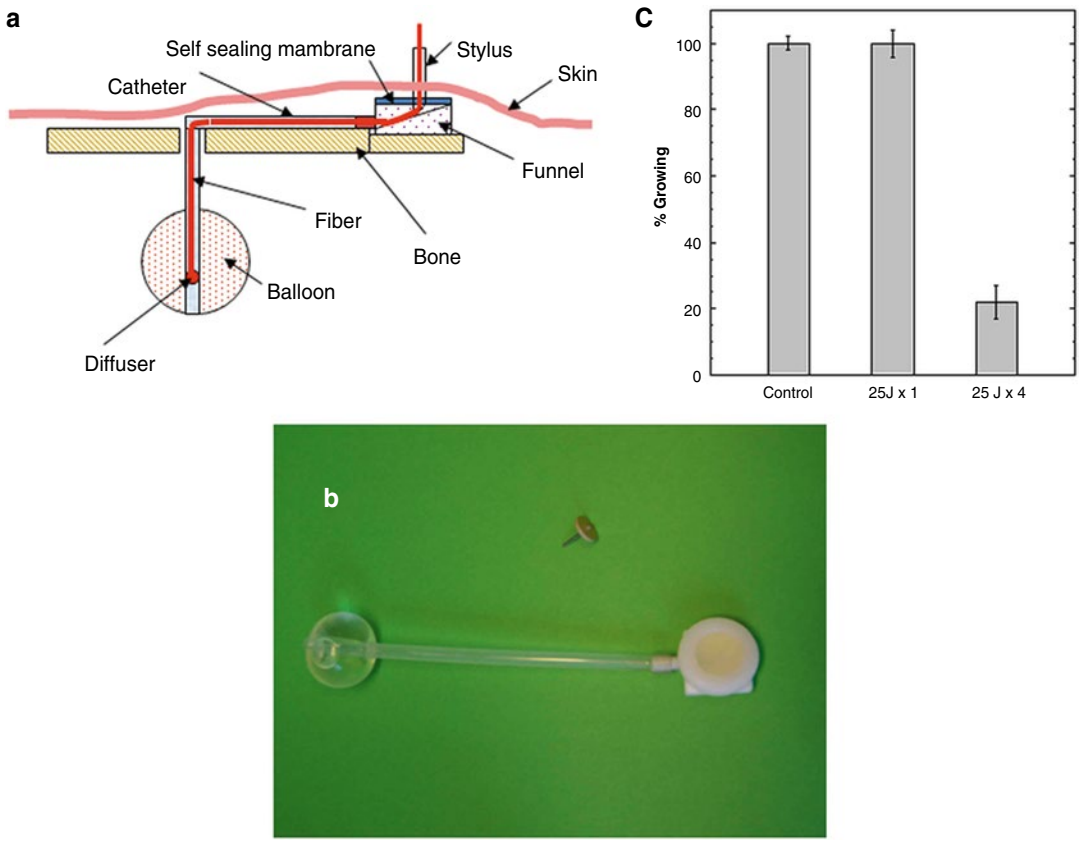

Fig. 4 Low dose-rate PDT. (**a**) Schematic and (**b**) photograph of indwelling balloon applicator for prolonged light delivery to the surgical resection cavity. The optical fiber is connected to a laser and the applicator is left in place following wound closure, (**c**) in vitro ALA-PDT responses in glioma spheroids showing suppression of spheroid growth following single low dose-rate (2.5 mW cm^{-2}) treatment or repetitive treatments (at weeks 0, 1, 2, and 3). Each data point represents % growth 12 weeks after the first treatment

Summary

PDT dosimetry is complex as it depends on a number of difficult-to-measure parameters. A further confounding factor is the dynamic interplay between these parameters. There are a number of established dosimetric techniques of varying degrees of complexity. The method chosen is typically dictated by the application and the level of physics support.

Widespread clinical acceptance of PDT will require strategies for accurate determination of the PDT dose. In contrast to radiation therapy, the dose is not measured directly in PDT—it is inferred from a number of indirect measurements including sensitizer photobleaching, oxygen perfusion, and light fluence rate. Direct dosimetry approaches involving measurement of the 1270 nm

singlet oxygen luminescence appear promising. Unfortunately, with current state-of-the-art singlet oxygen luminescence detection systems, the weak 1270 nm emission can only be measured at tissue surfaces. This limitation may be overcome with the development of fiber-coupled nanostructure detectors facilitating interstitial detection of singlet oxygen [101].

Rigorous PDT dosimetry approaches have been implemented recently in a number of clinical trials involving prostate cancer [61, 102] and basal cell carcinoma [62]. Such approaches, based on the principles discussed herein, may help establish PDT as a viable treatment option to radiation therapies such as the brachytherapy techniques used in the treatment of prostate cancer.

References

1. Raab O. Über die Wirkung fluoreszierender Stoffe and Infusorien. Z Biol. 1900;39: 524–46.
2. Dougherty TJ, Kaufman JE, Goldfarb A, Weisshaupt KR, Boyle D, Mittleman A. Photoradiation therapy for the treatment of malignant tumors. Cancer Res. 1978;38: 2628–35.
3. Dougherty TJ, Lawrence G, Kaufman JH. Photoradiation in the treatment of recurrent breast carcinoma. J Natl Cancer Inst. 1979;62:231–7.
4. Wilson BC, Patterson MS. The physics of photodynamic therapy. Phys Med Biol. 1986;31:327–60.
5. Wilson BC, Patterson MS. The physics, biophysics and technology of photodynamic therapy. Phys Med Biol. 2008;53:R61–109.
6. Hecht E. Optics. Reading, MA: Addison-Wesley; 1987.
7. Cheong W, Prahl SA, Welch AJ. A review of the optical properties of biological tissues. IEEE J Quant Electron. 1990;26:2166–85.
8. van de Hulst HC. Light scattering by small particles. New York: Dover; 1981.
9. Beer A, Lambert J. Einleitung in die höhere Optik. 1854.
10. Huppert TJ. History of diffuse optical spectroscopy of human tissue. In: Madsen SJ, editor. Optical methods and instrumentation in brain imaging and therapy. New York: Springer; 2013. p. 23–56.
11. Ishimaru A. Wave propagation and scattering in random media. New York: Academic; 1979. Ch 7 and 9.
12. Star WM. Diffusion theory of light transport. In: Welch AJ, van Gemert MJC, editors. Optical thermal response of laser-irradiated tissue. New York: Plenum; 1995. p. 131–206.
13. Henyey LG, Greenstein JL. Diffuse radiation in the galaxy. Astrophys J. 1941;93:70–83.
14. Chandrasekhar S. Radiative transfer. London: Oxford University Press; 1950.
15. Rybicki G. The searchlight problem with isotropic scattering. J Quant Spectros Radiat Transf. 1971;11:827–49.
16. Metropolis N, Ulam S. The Monte Carlo method. J Am Stat Assoc. 1949;44:335–41.
17. Wilson BC, Adam G. A Monte Carlo model for the absorption and flux distributions of light in tissue. Med Phys. 1983;10:824–30.
18. Flock ST, Patterson MS, Wilson BC, Wyman DR. Monte-Carlo modeling of light-propagation in highly scattering tissues. I. Model predictions and comparison with diffusion theory. IEEE Trans Biomed Eng. 1989;36:1162–8.
19. Farrell TJ, Patterson MS, Wilson BC. A diffusion theory model of spatially resolved, steady-state diffuse reflectance for the noninvasive determination of tissue optical properties *in vivo*. Med Phys. 1992;19:879–88.
20. Wang LH, Jacques SL, Zheng LQ. MCML—Monte Carlo modeling of light transport in multilayered tissues. Comput Methods Programs Biomed. 1995;47:131–46.
21. Zhu C, Liu Q. Review of Monte Carlo modeling of light transport in tissues. J Biomed Opt. 2013;18:050902.
22. Colasanti A, Guida G, Kisslinger A, Liuzzi R, Quarto M, Riccio P, Roberti G, Villani F. Multiple processor version of a Monte Carlo code for photon transport in turbid media. Comput Phys Commun. 2000;132:84–93.

23. Alerstam E, Svensson T, Andersson-Engels S. Parallel computing with graphic processing units for high-speed Monte Carlo simulation of photon migration. J Biomed Opt. 2008;13:060504.
24. Lo WCY, Redmond K, Lilge L, Luu J, Chow P, Rose J. Hardware acceleration of a Monte Carlo simulation for photodynamic therapy treatment planning. J Biomed Opt. 2009;14:014019.
25. Pratx G, Xing L. Monte Carlo simulation of photon migration in a cloud computing environment with MapReduce. J Biomed Opt. 2011;16:125003.
26. Barajas O, Ballangrud AM, Miller GG, Moore RB, Tulip J. Monte Carlo modeling of angular radiance in tissue phantoms and human prostate: PDT light dosimetry. Phys Med Biol. 1997;42:1675–87.
27. Liu B, Farrell TJ, Patterson MS. A dynamic model for ALA-PDT of skin: simulation of temporal and spatial distributions of ground-state oxygen, photosensitizer and singlet oxygen. Phys Med Biol. 2010;55:5913–32.
28. Valentine RM, Brown CTA, Moseley H, Ibbotson SH, Wood K. Monte Carlo modeling of *in vivo* protoporphyrin IX fluorescence and singlet oxygen production during photodynamic therapy for patients presenting with superficial basal cell carcinomas. J Biomed Opt. 2011;16:048002.
29. Valentine RM, Wood K, Brown CTA, Ibbotson SH, Moseley H. Monte Carlo simulations for optimal light delivery in photodynamic therapy of non-melanoma skin cancer. Phys Med Biol. 2012;57:6327–45.
30. Wyman DR, Patterson MS, Wilson BC. Similarity relations for the interaction parameters in radiation transport. Appl Opt. 1989;28:5243–9.
31. Star WM. Light dosimetry *in vivo*. Phys Med Biol. 1997;42:763–87.
32. Hull EL, Foster TH. Steady-state reflectance spectroscopy in the P_3 approximation. J Opt Soc Am A. 2001;18:584–99.
33. Patterson MS, Wilson BC, Wyman DR. The propagation of optical radiation in tissue. 1. Models of radiation transport and their application. Lasers Med Sci. 1991;6:155–68.
34. Kubelka P, Munk F. Ein beitrag zur optic der farbanstriche. Z Tech Phys. 1931;12:593–601.
35. Kubelka P. New contributions to the optics of intensely light scattering materials. J Opt Soc Am. 1948;38:448–57.
36. Prahl SA, van Gemert MJC, Welch AJ. Determining the optical properties of turbid media using the adding-doubling method. Appl Opt. 1993;32:559–68.
37. Pickering JW, Prahl SA, van Wieringen N, Beek JF, Sterenborg HJ, van Gemert MJC. Double-integrating-sphere system for measuring the optical properties of tissue. Appl Opt. 1993;32:339–410.
38. Pickering JW, Bosman S, Posthumus P, Blokland P, Beek JF, van Gemert MJC. Changes in the optical properties (at 632.8 nm) of slowly heated myocardium. Appl Opt. 1993;32:367–71.
39. Press WH, Teukolsky SA, Vetterling WT, Flannery BP. Numerical recipes in C: the art of scientific computing. New York: Cambridge University Press; 1992. p. 213–4.
40. Haskell RC, Svaasand LO, Tsay T-T, Feng T-C, McAdams MS, Tromberg BJ. Boundary conditions for the diffusion equation in radiative transfer. J Opt Soc Am A. 1994; 11:2727–41.
41. Kienle A, Patterson MS. Improved solutions of the steady-state and time-resolved diffusion equations or reflectance from a semi-infinite turbid medium. J Opt Soc Am A. 1997;14:246–54.
42. Hull EL, Nichols MG, Foster TH. Quantitative near-infrared spectroscopy of tissue-simulating phantoms containing erythrocytes. Phys Med Biol. 1998;43:3381–404.
43. Kienle A, Patterson MS, Dognitz N, Bays R, Wagnieres G, van den Bergh H. Noninvasive determination of the optical properties of two-layered turbid media. Appl Opt. 1998; 37:779–91.
44. Driver I, Lowdell CP, Ash DV. In vivo measurements of the optical interaction coefficients of human tumours at 630 nm. Phys Med Biol. 1991;36:805–13.
45. Li J, Zhu TC. Determination of *in vivo* light fluence distribution in a heterogeneous prostate during photodynamic therapy. Phys Med Biol. 2008;53:2103–14.
46. Patterson MS, Chance B, Wilson BC. Time resolved reflectance and transmittance for the non-invasive measurement of tissue optical properties. Appl Opt. 1989;28:2331–6.
47. Moulton JD. Diffusion theory modelling of picosecond laser pulse propagation in turbid media. M. Eng. Thesis, McMaster University, Hamilton, ON, Canada; 1990.
48. Madsen SJ, Wilson BC, Patterson MS, Park YD, Jacques SL, Hefetz Y. Experimental tests of a simple diffusion model for the estimation of scattering and absorption coefficients of turbid media from time resolved diffuse

reflectance measurements. Appl Opt. 1992;31:3509–17.

49. Fishkin J, Gratton E, vandeVen MJ, Mantulin WW. Diffusion of intensity modulated near-infrared light in turbid media. Proc SPIE. 1991;1431:122–35.
50. O'Leary MA, Boas DA, Chance B, Yodh AG. Refraction of diffuse photon density waves. Phys Rev Lett. 1992;69:2658–61.
51. Tromberg BJ, Svaasand LO, Tsay T-T, Haskell RC. Properties of photon density waves in multiple-scattering media. Appl Opt. 1993;32:607–16.
52. Patterson MS, Moulton JD, Wilson BC, Berndt KW, Lakowicz JR. Frequency-domain reflectance for the determination of the scattering and absorption properties of tissue. Appl Opt. 1991;30:4474–6.
53. Madsen SJ, Anderson ER, Haskell RC, Tromberg BJ. Portable, high-bandwidth frequency-domain photon migration instrument for tissue spectroscopy. Opt Lett. 1994;19:1934–6.
54. Pham TH, Coquoz O, Fishkin JB, Anderson E, Tromberg BJ. Broad bandwidth frequency domain instrument for quantitative tissue optical spectroscopy. Rev Sci Inst. 2000; 71:2500–13.
55. Redmond RW, Gamlin JN. A compilation of singlet oxygen yields from biologically relevant molecules. Photochem Photobiol. 1999;70:391–475.
56. Weishaupt KR, Gomer CJ, Dougherty TJ. Identification of singlet oxygen as cytotoxic agent in photoinactivation of a murine tumor. Cancer Res. 1976;36:2326–9.
57. Niedre M, Patterson MS, Wilson BC. Direct near-infrared luminescence detection of singlet oxygen generated by photodynamic therapy in cells *in vitro* and tissues *in vivo*. Photochem Photobiol. 2002;75:382–91.
58. Foote CS. Definition of type-I and type-II photosensitized oxidation. Photochem Photobiol. 1991;54:659.
59. Farrell TJ, Wilson BC, Patterson MS, Olivo MC. Comparison of the *in vivo* photodynamic threshold dose for Photofrin, mono- and tetrasulfonated aluminum phthalocyanine using a rat liver model. Photochem Photobiol. 1998;68:394–9.
60. Wilson BC, Patterson MS, Lilge L. Implicit and explicit dosimetry in photodynamic therapy: a new paradigm. Lasers Med Sci. 1997; 12:182–99.
61. Weersink RA, Bogaards A, Gertner M, Davidson SR, Zhang K, Netchev G, Trachtenberg J, Wilson BC. Techniques for delivery and monitoring of TOOKAD (WST09)-mediated photodynamic therapy of the prostate: clinical experience and practicalities. J Photochem Photobiol B. 2005; 79:211–22.
62. Thompson MS, Johansson A, Johansson T, Andersson-Engels S, Svanberg S, Bendsoe N, Svanberg K. Clinical system for interstitial photodynamic therapy with combined on-line dosimetry measurements. Appl Opt. 2005;44:4023–31.
63. Zhu TC, Finlay JC, Hahn SM. Determination of the distribution of light, optical properties, drug concentration, and tissue oxygenation *in vivo* in human prostate during motexafin lutetium-mediated photodynamic therapy. J Photochem Photobiol B. 2005;79:231–41.
64. Zeng H, Korbelik M, McLean DI, MacAulay C, Lui H. Monitoring photoproduct formation and photobleaching by fluorescence spectroscopy has the potential to improve PDT dosimetry with a verteporfin-like photosensitizer. Photochem Photobiol. 2002;75:398–405.
65. Georgakoudi I, Nichols MG, Foster TH. The mechanism of Photofrin photobleaching and its consequences for photodynamic dosimetry. Photochem Photobiol. 1997;65:135–44.
66. Robinson DJ, de Bruijn HS, van der Veen N, Stringer MR, Brown SB, Star WM. Fluorescence photobleaching of ALA-induced protoporphyrin IX during photodynamic therapy of normal hairless mouse skin: the effect of light dose and irradiance and the resulting biological effect. Photochem Photobiol. 1998;67:140–9.
67. Diamond KR, Patterson MS, Farrell TJ. Quantification of fluorophore concentration in tissue-simulating media by fluorescence measurements with a single optical fiber. Appl Opt. 2003;42:2436–42.
68. Pogue BW, Burke G. Fiber-optic bundle design for quantitative fluorescence measurement from tissue. Appl Opt. 1998;37:7429–36.
69. Farrell TJ, Patterson MS, Hayward JE, Wilson BC, Beck ER. A CCD and neural network based instrument for the non-invasive determination of tissue optical properties *in vivo*. Proc SPIE. 1994;2135:117–28.
70. Synytsya A, Kral V, Matejka P, Pouckova P, Volka K, Sessler JL. Biodistribution assessment of a lutetium (III) texaphyrin analogue in tumor-bearing mice using NIR Fourier-transform Raman spectroscopy. Photochem Photobiol. 2004;79:453–60.

71. Buerk DG. Measuring tissue PO_2 with microelectrodes. Methods Enzymol. 2004;381: 665–90.
72. Papkovsky DB. Methods in optical oxygen sensing: protocols and critical analyses. Methods Enzymol. 2004;381:715–35.
73. Braun RD, Lanzen JL, Snyder SA, Dewhirst MW. Comparison of tumor and normal tissue oxygen tension measurements using OxyLite or microelectrodes in rodents. Am J Physiol Heart Circ Physiol. 2001;280:H2533–44.
74. Dysart JS, Patterson MS. Characterization of Photofrin photobleaching for singlet oxygen dose estimation during photodynamic therapy of MLL cells *in vitro*. Phys Med Biol. 2005;50:2597–616.
75. Jarvi MT, Patterson MS, Wilson BC. Insights into photodynamic therapy dosimetry: simultaneous singlet oxygen luminescence and photosensitizer photobleaching measurements. Biophys J. 2012;102:661–71.
76. Finlay JC, Mitra S, Patterson MS, Foster TH. Photobleaching kinetics of Photofrin *in vivo* and in multicell tumor spheroids indicate two simultaneous bleaching mechanisms. Phys Med Biol. 2004;49:4837–60.
77. Dysart JS, Patterson MS. Photobleaching kinetics, photoproduct formation, and dose estimation during ALA induced PpIX PDT of MLL cells under well oxygenated and hypoxic conditions. Photochem Photobiol Sci. 2006;5:73–81.
78. Rodgers MAJ. On the problem involved in detecting the luminescence from singlet oxygen in biological specimens. J Photochem Photobiol B Biol. 1988;1:371–3.
79. Patterson MS, Madsen SJ, Wilson BC. Experimental tests of the feasibility of singlet oxygen luminescence monitoring *in vivo* during photodynamic therapy. J Photochem Photobiol. 1990;5:69–84.
80. Gorman AA, Rodgers MAJ. Current perspectives of singlet oxygen detection in biological environments. J Photochem Photobiol B Biol. 1992;14:159–76.
81. Hirano T, Kohno E, Nishiwaki M. Detection of near infrared emission from singlet oxygen in PDT with an experimental tumor bearing mouse. J Jpn Soc Laser Surg Med. 2002;22:99–108.
82. Niedre MJ, Secord AJ, Patterson MS, Wilson BC. *In vitro* tests of the validity of singlet oxygen luminescence measurements as a dose metric in photodynamic therapy. Cancer Res. 2003;63:7986–94.
83. Niedre MJ, Yu CS, Patterson MS, Wilson BC. Singlet oxygen luminescence as an *in vivo* photodynamic therapy dose metric: validation in normal mouse skin with topical aminolevulinic acid. Br J Cancer. 2005;92:298–304.
84. Jimenez-Banzo A, Ragas X, et al. Time-resolved methods in biophysics. 7. Photon counting vs. analog time-resolved singlet oxygen phosphorescence detection. Photochem Photobiol Sci. 2008;7:1003–10.
85. Luna MC, Wong S, Gomer CJ. Photodynamic therapy mediated induction of early response genes. Cancer Res. 1994;54:1374–80.
86. Oleinick NL, Evans HH. The photobiology of photodynamic therapy: cellular targets and mechanisms. Radiat Res. 1998;150:S146–56.
87. Veenhuizen RB, Stewart FA. The importance of fluence rate in photodynamic therapy—is there a parallel with ionizing radiation dose-rate effects. Radiother Oncol. 1995;37:131–5.
88. Sterenborg HJCM, vanGemert MJC. Photodynamic therapy with pulsed light sources: a theoretical analysis. Phys Med Biol. 1996;41:835–49.
89. Tromberg BJ, Orenstein A, Kimel S, Barker SJ, Hyatt J, Nelson JS, Berns MW. *In vivo* tumor oxygen-tension measurements for the evaluation of the efficiency of photodynamic therapy. Photochem Photobiol. 1990;52: 375–85.
90. Foster TH, Murant RS, Bryant RG, Knox RS, Gibson SL, Hilf R. Oxygen consumption and diffusion effects in photodynamic therapy. Radiat Res. 1991;126:296–303.
91. Foster TH, Gao L. Dosimetry in photodynamic therapy—oxygen and the critical importance of capillary density. Radiat Res. 1992;130:379–83.
92. Busch TM. Local physiological changes during photodynamic therapy. Lasers Surg Med. 2006;38:494–9.
93. Chen Q, Chen H, Hetzel FW. Tumor oxygenation changes post-photodynamic therapy. Photochem Photobiol. 1996;63: 128–31.
94. Chen Q, Huang Z, Chen H, Shapiro H, Beckers J, Hetzel FW. Improvement of tumor response by manipulation of tumor oxygenation during photodynamic therapy. Photochem Photobiol. 2002;76:197–203.
95. Henderson BW, et al. Photofrin photodynamic therapy can significantly deplete or preserve oxygenation in human basal cell carcinomas during treatment depending on fluence rate. Cancer Res. 2000;60:525–9.
96. Coutier S, Bezdetnaya LN, Foster TH, Parache RM, Guillemin F. Effect of irradiation fluence rate on the efficacy of photodynamic therapy and tumor oxygenation in meta-

tetra(hydroxyphenyl)chlorine (mTHPC)-sensitized HT29 xenografts in nude mice. Radiat Res. 2002;158:339–45.

97. Henderson BW, Gollnick SO, Snyder JW, Busch TM, Kousis PC, Cheney RT, Morgan J. Choice of oxygen-conserving treatment regimen determines the inflammatory response and outcome of photodynamic therapy in tumors. Cancer Res. 2004;64: 2120–6.
98. Bisland SK, Lilge L, Lin A, Rusnov R, Wilson BC. Metronomic photodynamic therapy as a new paradigm for photodynamic therapy: rationale and pre-clinical evaluation of technical feasibility for treating malignant brain tumors. Photochem Photobiol. 2004;80: 2–30.
99. Madsen SJ, Sun C-H, Tromberg BJ, Hirschberg H. Development of a novel indwelling balloon applicator for optimizing light delivery in photodynamic therapy. Lasers Surg Med. 2001;29:406–12.
100. Madsen SJ, Sun C-H, Tromberg BJ, Hirschberg H. Repetitive 5-aminolevulinic acid-mediated photodynamic therapy on human glioma spheroids. J Neurooncol. 2003;62:243–50.
101. Gemmell NR, McCarthy A, Liu B, Tanner MG, Dorenbos SD, Zwiller V, Patterson MS, Buller GS, Wilson BC, Hadfield RH. Singlet oxygen luminescence detection with a fiber-coupled superconducting nanowire single-photon detector. Opt Express. 2013;21: 5005–13.
102. Du KL, Mick R, Busch TM, Zhu TC, Finlay JC, Yu G, Yodh AG, Malkowicz SB, Smith D, Whittington R, Stripp D, Hahn SM. Preliminary results of interstitial motexafin lutetium-mediated PDT for prostate cancer. Lasers Surg Med. 2006;38:427–34.